Intraseasonal variability of winter precipitation over Central Asia and the Western Tibetan plateau from 1979 to 2013 and its relationship with the North Atlantic Oscillation

Intraseasonal Variability of Winter Precipitation over Central Asia and the Western Tibetan Plateau from 1979 to 2013 and its Relationship with the North Atlantic Oscillation

Heng Liu[a, b*], Xiaodong Liu[a, b, c], Buwen Dong[d]

[a] SKLLQG, Institute of Earth Environment, Chinese Academy of Sciences, Xi'an, 710061, China
[b] College of Earth Science, University of Chinese Academy of Sciences, Beijing, 100049, China
[c] CAS Center for Excellence in Tibetan Plateau Earth Sciences, Beijing, 100101, China
[d] National Centre for Atmospheric Science, University of Reading, Reading, RG6 6BB, UK

Abstract

Winter precipitation over Central Asia and the western Tibetan Plateau (CAWTP) is mainly a result of the interaction between the westerly circulation and the high mountains around the plateau. Empirical Orthogonal Functions (EOFs), Singular Value Decomposition (SVD), linear regression and composite analysis were used to analyze winter daily precipitation and other meteorological elements in this region from 1979 to 2013,in order to understand how interactions between the regional circulation and topography affect the intraseasonal variability in precipitation. The SVD analysis showed that the winter daily precipitation variability distribution is characterized by a dipole pattern with opposite signs over the northern Pamir Plateau and over the Karakoram Himalaya, similar to the second mode of EOF analysis. This dipole pattern of precipitation anomaly is associated with local anomalies in both the 700hPa moisture transport and the 500hPa geopotential height and is probably caused by oscillations in the regional and large-scale circulations, which can influence the westerly disturbance tracks and water vapor transport. The linear regression showed that the anomalous mid-tropospheric circulation over CAWTP corresponds to an anti-phase variation

* Corresponding author. E-mail address: liuheng@ieecas.cn

of the 500 hPa geopotential height anomalies over the southern and northern North Atlantic 10 days earlier (at 95% significance level), that bear a similarity to the North Atlantic Oscillation (NAO). The composite analysis revealed that the NAO impacts the downstream regions including CAWTP by controlling south-north two branches of the middle latitude westerly circulation around the Eurasian border. During the positive phases of the NAO, the northern branch of the westerly circulation goes around the northwest Tibetan Plateau, whereas the southern branch encounters the southwest Tibetan Plateau, which leads to a reduced precipitation over the northern Pamir Plateau and an increased precipitation over the Karakoram Himalaya, and vice versa.

KEY WORDS: Topographic precipitation; North Atlantic Oscillation; Westerly circulation; Statistical analysis; Intraseasonal variability.

1 Introduction

The geographical region covered by Central Asia and the western Tibetan Plateau (CAWTP, 30–45° N, 60–85° E) has complex terrains and a unique climate. The Turan Depression is located in the northwest, whereas the high mountains and plateaus (e.g. the Iran Plateau, the Hindu Kush, the Karakoram Himalaya, the Pamir Plateau and the Tian Shan mountains) are located from the southwest to the northeast (Fig. 1). The CAWTP region has an arid to semiarid climate with an annual precipitation less than 400 mm, except for a few of the high mountain areas. Because of the scarcity of water resources, there is a high risk that global climate change will threaten both the natural environment and the human population in this region (Ragab &

Prudhomme 2002, WB et al. 2009).

Despite the complex topography and lack of meteorological stations, satellite remote sensing data have been used to determine the spatiotemporal distribution of precipitation over Central Asia (Guo et al. 2015) and the western Tibetan Plateau (Pohl et al. 2015). High-resolution regional climate models have also been used to determine the patterns of precipitation over CAWTP (Small et al. 1999, Schiemann et al. 2008, Ozturk et al. 2012, Maussion et al. 2014).

Previous studies have reported the spatiotemporal distribution and regional differences in precipitation over CAWTP and have found that the major weather system controlling the winter precipitation over CAWTP is the westerly circulation (Schiemann et al. 2009, Yin et al. 2014). In winter, the westerly circulation transports moisture to Central Asia (Bothe et al. 2012), southwest Asia (Malik et al. 2015) and the western Tibetan Plateau (Curio et al. 2015). The westerly circulation is disturbed by the high mountains in this region and causes heavy precipitation and storms over the Pamir Plateau, the Hindu Kush, the Karakoram Himalaya and the western Himalaya (Lang & Barros 2004, Cannon et al. 2015a, b). Yin et al. (2014) compared the differences in precipitation climatology between the arid area of Central Asia and the East Asia monsoon region and showed that winter is the rainy season in Central Asia, whereas the rainy season occurs in summer for East Asia. They further showed that the control atmospheric circulation over the western area changes between winter and summer. In winter it is dominated by westerly upper-air flows, bringing moisture from the upstream to the region while in summer it is dominated by northeasterly winds from the Asian interior, resulting in a

dry condition. The westerly circulation is not only the major weather system controlling the winter mean precipitation over CAWTP, but also precipitation interannual variability and trend in the region (Chen et al. 2011, Yin et al. 2014, Cannon et al. 2015a).

There have been many reports that large-scale atmospheric teleconnections regulate the mid-latitude westerly circulation variability which in turn may influence interannual precipitation variation over CAWTP (e.g. Aizen et al. 2001, Syed et al. 2006, Mariotti 2007, Filippi et al. 2014, Yin et al. 2014, Cannon et al. 2015a, b, Hoell et al. 2015). Although some evidence has been found that at interannual time scale the El Niño–Southern Oscillation may be related to the precipitation variation in the cold season over Central and Western Asia (Mariotti 2007, Hoell et al. 2015), other research has shown a close relationship between the winter interannual precipitation variation over CAWTP and the North Atlantic Oscillation (NAO) (Aizen et al. 2001, Syed et al. 2006, 2010, Yadav et al. 2009, Filippi et al. 2014, Yao and Chen 2015). Aizen et al. (2001) analyzed the relationship between mid-latitude precipitation in Asia and the large-scale circulation of the atmosphere using data from hydro-meteorological stations. Their results showed more precipitation over the Pamir and Tian Shan mountains during the positive phases of the NAO. Syed et al. (2006) found a positive precipitation anomaly over northwestern Asia that is well matched with the positive phase of the NAO. Syed et al. (2010) presented a regional climate modeling study on both NAO and ENSO and discussed the influence of westerly disturbances. Filippi et al. (2014) verified that winter interannual precipitation variation over the Hindu Kush–Karakoram Himalaya region is affected by the NAO. During the positive phases of the NAO, the Middle East, which is

upstream of CAWTP, experiences stronger westerly winds and evaporation, which leads to an enhanced moisture transport and therefore enhanced precipitation over the Hindu Kush. Yao and Chen (2015) found a significant negative correlation between the yearly precipitation on mountains of the Syr Darya River Basin and NAO index from 1891 to 2011 but it turned out non-significant on plains.

Previous studies have mainly considered the interannual variation in winter precipitation over a specific area and its connection with the NAO and other large-scale circulations (e.g. Aizen et al. 2001, Syed et al. 2006, Mariotti 2007, Filippi et al. 2014, Yin et al. 2014, Cannon et al. 2015a, Hoell et al. 2015). However, little attention has been paid to the spatiotemporal distribution of precipitation variability over CAWTP at the intraseasonal time scale. Therefore it is important to investigate the spatial and temporal distribution of winter precipitation variation over CAWTP on this time scale, to analyze its connection with regional and large-scale circulations and to elucidate physical processes involved by using daily precipitation data and other meteorological parameters.

2 Data and methods

Daily precipitation data from the Climate Prediction Center (Chen et al. 2008) and daily meteorological variables of ERA-Interim from the European Centre for Medium-Range Weather Forecasts (Dee et al. 2011) were used in this study. Sapna Rana (2017) have already used the CPC Unified Rain gauge data and compared it with 9 other precipitation products over the central southwest Asia. Their results show that the CPC data can reasonably reflect

the spatial-temporal distribution of winter precipitation over CAWTP despite some systematic differences in the time means The used ERA-Interim variables include the daily 700 and 500 hPa geopotential height, meridional and zonal winds, the total column of water vapor (TCWV) and the mean sea level pressure. The horizontal resolution of all the data is 0.5°longitude × 0.5° latitude. In consideration of the higher accuracy of the reanalysis data obtained over high mountain areas after 1979, when satellite data were first applied (Cannon et al. 2015b), we chose all winters (December-March), consistent with other studies analyzing the relationships between teleconnection patterns and precipitation in this area (Syed et al. 2006, 2010, Yadav et al. 2009, Filippi et al. 2014) from 1979 to 2013, a total of 4244 days, as the study period. The daily average data were obtained from four records with a six-hour interval for each day. The encounter of westerly wind with high mountains of Tibetan Plateau happened around 700 hPa , which is closely connected with topographic precipitation, and therefore 700 hPa wind is used to indicate low tropospheric circulation. The 500hPa geopotential height anomaly can indicate the teleconnections.

To determine the characteristics of the winter intraseasonal precipitation and circulation variability in CAWTP, the climatological seasonal cycle from December to the next March in the daily data was removed before the analysis. We averaged the data of the same date of all the years (1979-2013) and then calculated the 21 day moving mean as the climate mean state. Thus, the daily values with climatological seasonal cycle removed were obtained by subtracting the climate mean state from the actual data according to the following formula:

$$Z_n^* = Z_n - \Big(\sum_{i=-10,10} \big(\sum_{j=1,35} Z_{k+(i-1)\times 365+j} \big) / 35 \Big) / 21$$

where n is the number of days from December 1, 1979; k is the number of days from December 1 of a specific year; i is the number of years from 1979; j is the day from 10 days before to 10 days after a specific day; and Z_n^* is the value after removing the climatological seasonal cycle.

The EOF analysis was used to decompose winter daily precipitation variability over CAWTP to find the spatial patterns as well as their time variation (Bjornsson and Venegas 1997). Figure 1 shows the study area with 1581 grid boxes and 4244 day time series at each grid box, which is the basis for the EOF analysis.

Singular value decomposition (SVD) analysis (Wallace et al. 1992) was applied to show the spatiotemporal relationship between the winter daily precipitation and the regional circulation variations over CAWTP. This method identifies a pair of covaried spatial patterns, their temporal variations and the covariance between two variables (Bjornsson and Venegas 1997).

Lead-lag linear regression was applied to study the connection between the 500 hPa geopotential height variability over CAWTP and the upstream westerly jet variability (Wang and Zhang 2015).

We also constructed composites of the precipitation distribution in CAWTP during positive and negative NAO cases respectively, and discussed the relationship between the NAO and the precipitation variability at the intraseasonal time scale. The NAO index was defined as the standardized difference in mean sea level pressure between the southern North Atlantic (25°–40°N, 50°–10°W) and the northern North Atlantic (50°–65°N, 10°–50°W)

(Hurrell 1996). After calculating the daily index for every winter from 1979 to 2013, the central day of a positive (negative) NAO phase event was defined as the day with the relative maximum (minimum) value of the NAO index in continuous five days and being greater (less) than 1.5 (-1.5) at the same time. In this way, a total of 85 positive NAO phase cases and 82 negative phase cases were selected for the composites. Here we did composite analysis based on cases with strong NAO anomalies in order to see teleconnections between two regions and significant NAO related remote climatic anomalies over CAWTP. To trace westerly wind disturbance (WWD) tracks, a wave-tracking approach was applied as documented in Cannon (2015b) who defined the centers of the disturbances by standardized 500 hPa geopotential height anomaly and a set of spatial threshold and temporal correlation to identify the tracks. Here we used the 500hPa geopotential height anomaly of 1 standard deviation and the spatial extent of 5 degrees as a set of thresholds to identify the location of centers to count the WWDs. Then the WWD frequency in every grid was calculated.

3 Spatial and temporal distribution of winter precipitation over CAWTP and its connection with the contemporaneous regional circulation

3.1 Winter precipitation climatology over CAWTP

The climate of Central Asia is controlled on an annual basis by westerly winds containing little moisture, and it is classified as a typical arid to semiarid region. The rainy season usually occurs in winter (from December to March) (Yin et al. 2014) and most of the moisture transported by the strong westerly winds is intercepted to condense by the high mountains

of the region during this period (Syed et al. 2006). Figure 2a shows the spatial distribution of the winter mean climatological precipitation over Asia from 1979 to 2013. There is more precipitation over CAWTP and the main areas of precipitation are distributed on the windward slope of the western Tibetan Plateau, in agreement with earlier reports by Schiemann et al. (2008) and Yin et al. (2014). There are two core areas of precipitation centered at 70°E, 42°N and 75°E, 33°N respectively, with the maximum precipitation rate of 8 mm d^{-1}. The winter precipitation over CAWTP accounts for more than 50% of the annual precipitation (Fig. 2b). The distribution of water vapor flux integrated vertically from 950 hPa to 300 hPa (Fig. 2c) suggests that the moisture transport convergence over CAWTP is mainly controlled by mid-tropospheric westerly winds, rather than by lower-tropospheric (below 950 hPa) circulations (not shown). The distribution of WWD frequency (Fig. 2d) shows that more WWDs occur in the Karakoram Himalaya, coincident with the local precipitation maximum there shown in Fig. 2a. This is consistent with Cannon et al. (2015a, b) who reported that heavy precipitation occurs when the WWD encountered mountains of the Himalaya. The climatology of precipitation over CAWTP is quite different from that over the monsoon areas. The annual precipitation over CAWTP is much lower than that over Asian monsoon regions and mainly occurs in winter, when the mountains block and lift the strong mid-latitude westerly circulation (e.g., Yin et al 2014, Cannon et al. 2015a, b).

3.2 Intraseasonal variability in winter daily precipitation and circulation over CAWTP

It is possible that the strength and position of westerly circulation determine the forced

upward motion, frequency of WWDs and the distribution of precipitation on the intraseasonal time scale. The winter daily precipitation was decomposed by EOF analysis after the climatological seasonal cycle was removed and the first two modes are shown in Fig. 3a and 3b. The first mode shows the same sign allover CAWTP with explained variance of 24.4% and the second mode shows a seesaw pattern between northern Pamir Plateau and the Karakoram Himalaya with explained variance of 15.6%. These EOF modes suggest the existence of the intraseasonal variability of winter precipitation over CAWTP. Then we composited the 500 hPa zonal wind (U component) during the dominant periods according to the time series of the first mode and the second mode as Fig. 3c and Fig. 3d, which indicated close connection between regional circulation and precipitation. Therefore, the relationship between the regional circulation and precipitation in the study area is explored in the following.

The seasonal cycle removed daily precipitation and 700hPa moisture flux fields for 35 winters during 1979–2013 were used for the SVD analysis to determine the simultaneous relationship between the precipitation and circulation variability over CAWTP. The first SVD mode shows a dipole pattern of precipitation variability with a positive anomaly over the Karakoram Himalaya (center located at 33°N, 78°E, Fig.4a) and a negative anomaly over the northern Pamir Plateau (center located at 40°N, 68°E), bearing a very similar structure as shown for the second mode of EOF analysis (Fig. 3b). Accompanied with this pattern of precipitation variability is a southerly wind anomaly over the Karakoram Himalaya and a northwesterly wind anomaly (southwesterly wind weakened) over the northern Pamir

Plateau(not shown) and anomalous lower tropospheric moisture transport (Fig. 4b). This pattern of precipitation anomaly is closely related to the forced lifting of the westerly airstream on the windward side of the mountains. The explained variance reaches 55.12% and the correlation coefficient between the time coefficients of two fields is 0.65 for the first SVD mode, suggesting the importance of orographic forcing in modulating the regional precipitation at the intraseasonal time scale.

We also did the SVD analysis with the seasonal cycle removed daily precipitation and 500 hPa geopotential height fields over CAWTP. The explained variance and correlation coefficient corresponding for the first SVD mode are 60.5% and 0.64, respectively (Fig. 4c and d). Figs. 4c and 4d illustrate that a negative center over the southeast of CAWTP in the field of 500 hPa geopotential height anomaly is associated with a precipitation anomaly pattern with the wetter southeast and the drier northwest. Hence, the distribution of winter precipitation anomaly in the study area at the intraseasonal time scale is the result of topography-affected regional atmospheric circulation variability. In the following, a lead-lag linear regression was used to further reveal the relationship between the regional and large-scale circulation variations and the regional precipitation change.

4 Correlation of 500hPa geopotential height over CAWTP with the preceding atmospheric circulation over the North Atlantic Ocean and Eurasia

The preceding atmospheric circulation over the Atlantic Ocean and Eurasian region may influence the regional circulation over CAWTP, leading to the regional precipitation anomaly

via teleconnection. The time series of the 500 hPa geopotential height analyzed by SVD was normalized and then the normalized time series with an absolute value greater than 1.5 and higher than the neighboring 4 other days was chosen for further analysis (a total of 200 time series mixed with both positive and negative values). A linear regression was applied between the chosen 200 time series and the antecedent 500 hPa geopotential height field over the Atlantic Ocean–Eurasian region from lead 16 days to the lag 3 day of the chosen days respectively and results are shown in figure 5. There is a positive geopotential height anomaly over the Azores (center located at 30°W and 40°N) and a negative anomaly over Iceland (center located at 10°W and 60°N) from day −10 to day −8 (10 to 8 days before the regional circulation phase, the same below) (Fig. 5a, 5b). These patterns of the anomalous circulation show a similarity to the positive phase of the NAO (Hurrell 1996). On day −6, the original negative geopotential height anomaly over Iceland moves to the east and a significant positive anomaly occurs over the Eurasian border and northern Asia and meanwhile a negative anomaly over CAWTP develops (Fig. 5c). With time advance, the magnitude of the anomaly over the Atlantic Ocean decrease, whereas the strength of the anomalies over the Eurasian border and over CAWTP enhance on day −4 (Fig. 5d). On day −2 and 0, significant negative geopotential height anomalies occur over CAWTP (Fig. 5e, 5f), similar to the results of the SVD analysis. It is therefore possible that the regional circulation has been affected by the preceding large-scale circulation variability related to NAO.

The time evolution of the 500hPa geopotential height anomaly over the North Atlantic was analyzed by lead-lag linear regression and correlation. Areas A (20–40° W, 30–40° N), B

(0–20° W, 54–64° N), C (44–64° E, 54–64° N) and D (60–80° E, 30–40° N) in Fig. 5 were chosen to calculate the average geopotential height anomaly and the correlation coefficient in different lead days. The four domains are recognized in consideration of both covering the centers of 500hPa geopotential height anomaly and the significant at 95% level in Fig. 5. Otherwise, the numbers of the grids of the four domains should be the same so they are comparable. Table 1 lists regression coefficients and correlation coefficients of regionally-averaged 500 hPa geopotential heights on different lag days for these four areas and the time coefficients of the first mode of 500 hPa geopotential height field over CAWTP in the above SVD analysis. From days −15 to −9 (the negative number means the days before the day for the regional SVD analysis) there is a positive anomaly over area A, a significant increasingly negative anomaly over area B, and no significant anomaly over area C. From days −8 to −4, the anomaly over area A decreases and the anomaly over area B increases to a maximum value. A significant positive anomaly appears over area C on day −5 and increases rapidly afterwards. From days −3 to 0 there is no significant anomaly over area A, the anomaly over area B decreases, and the anomaly over areas C and D increases to maximum values. From days +1 to +3 there is no significant anomaly over area B and the anomaly over areas C and D decreases. Figure 5 and Table 1 show time evolutions of geopotential height anomaly in various regions before the maximum height anomaly over CAWTP and suggest that NAO-like circulation anomaly over the North Atlantic is a precursor for the intraseasonal variation of precipitation over CAWTP. The lead-lag correlation coefficients between NAO index and time series of first SVD mode in these chosen days were calculated and they are given in Table 1.

These correlation coefficients indicate large correlations when NAO leads the regional geopotential height by about 10 days.

Although we found a close connection between the 500 hPa geopotential height over CAWTP and geopotential height over the North Atlantic about 10-8 days before by linear regression and correlation, further analysis was required to elucidate the mechanism for the relationship between the north–south precipitation seesaw over CAWTP during both positive and negative NAO phases respectively. In the following, composite analysis was therefore used to further investigate how the different NAO phases influenced the regional circulation and precipitation over CAWTP.

5 Influence of the NAO on spatial and temporal distribution of winter precipitation over CAWTP

Based on our definition of NAO events, the 500 hPa geopotential height, the 700 hPa wind flow field were combined to assess the influence of the NAO on the circulation over remote downstream areas. The time evolutions of composited 500hPa geopotential height anomaly and 700 hPa streamlines at different lags for the positive and negative NAO phase cases are illustrated in Fig. 6. In positive NAO phases, the NAO pattern is clearly shown on the 0 day (the peak day of NAO index) with the strong negative 500 hPa geopotential height anomaly over the Iceland and the positive one over the Azores. As time advances, the positive anomaly extends eastward to the Eurasian border. In the following days, NAO pattern is weakening and the east positive anomaly is further extended eastward and is finally separated from the

positive anomaly over the Azores. The eastward extension of positive anomaly over the Eurasian border is associated with the intensification of the negative anomaly over the CAWTP (Fig. 6c). The time evolutions of the 700 hPa wind streamlines associated with geopotential height anomaly evolutions offer another view. Associated with positive NAO at day 0 is a single strong westerly jet over the North Atlantic and two branches of strong westerly wind, whose axes locate on 55°N and 30°N along the Eurasian border, resulted from the positive 500 hPa geopotential height anomaly over the Eurasian border (Fig. 6a). Over the Eurasian border, the north branch westerly wind forms a ridge while the south one forms a trough. They both extend eastward in a similar way as the positive 500 hPa geopotential height anomaly. The north branch westerly wind goes around the north CAWTP while the south branch encounters the Karakoram Himalaya. The Figs. 6d, 6e and 6f show time evolutions of composited 500hPa geopotential height anomaly and 700 hPa streamlines at different days for the negative NAO phases. Time evolutions of geopotential height anomaly show similar evolutions as those during the positive NAO phase cases, but with a change in sign of the anomalies. Associated with the negative NAO phases, the north branch of westerly wind encounters the north CAWTP while the south branch goes around the Krakoram-Himalaya at day 10.

The time averaged 700 hPa moisture flux anomaly and WWD frequency anomaly from day 5 to day 10 after the peak of NAO phases intuitively show the regulation of regional circulation by the NAO. During the positive NAO phases, northeasterly moisture flux anomalies (decreased southwesterly moisture flux) occur over the Central Asia and northern Pamir Plateau, whereas southerly moisture flux anomalies accompanied with higher

frequency of WWD occur over the Karakoram Himalaya (Fig. 7a). During the negative NAO phases, southwesterly moisture flux anomalies occur over the Central Asia and northern Pamir Plateau, whereas northeasterly moisture flux anomalies accompanied with lower frequency of WWD occur over the Karakoram Himalaya (Fig. 7b). The composites of precipitation anomalies of positive and negative NAO phases, as shown in Fig. 7c and 7d, are well matched with the regional circulation and moisture flux anomalies. There is less precipitation over the north east of Iran, Turkmanistan, Tajikistan and Kyrgyzstan (center at ~ 75°E, 34°N) and more precipitation over the Karakoram Himalaya (center at ~ 70°E, 42°N) during positive NAO phases and vice versa. For the south part, the WWD seems to be more important while the moisture flux takes control of the north part. Compared with the daily average winter precipitation (Fig. 2a), the precipitation anomaly at the intraseasonal time scale reaches 10% of the climatological mean. The precipitation composites during the different NAO phases are similar to the results of the SVD analyses. The two analyses both demonstrate the teleconnection between the NAO over the North Atlantic and the regional circulation and precipitation variability over CAWTP.

6 Discussion and conclusions

The climate is characterized by dominant westerly circulation and scarce precipitation over CAWTP. The lowlands of this area are almost rainless due to the lack of moisture and upward motion. By contrast, heavy rains occur on the high mountain areas as a result of the uplifting of the westerly winds by the high topography.

There have been much published research on precipitation and its interannual variability over the Karakoram Himalaya (Syed et al. 2006, 2010, Filippi et al. 2014, Cannon et al. 2015a, b). For example, Cannon et al. (2015a, b) stressed the importance of the westerly disturbance. Less research has focused on precipitation over the northern Pamir Plateau and mainly focuses on interannual variations (e.g., Chen et al. 2011). Filippi et al. (2014) and Syed et al. (2006) found that the interannual variation in precipitation is connected to the NAO, but they did not discuss the intraseasonal precipitation variations and the contemporaneous opposite variations over the northern Pamir Plateau and over the Karakoram Himalaya.

This study focused on the intraseasonal variation in winter daily precipitation over CAWTP. The EOF, SVD, lead-lag linear regression and composite analyses showed that a seesaw pattern of winter intraseasonal precipitation anomaly between the Karakoram Himalaya and the northern Pamir Plateau is connected with the intraseasonal oscillation of the NAO. The main physical processes for the seasaw pattern of precipitation variability are the trough–ridge phase of the two westerly jets rather than the westerly strength at the intraseasonal scale. Multi-method analyses gave similar results, confirming that the NAO is able to influence the intraseasonal precipitation variability in winter over CAWTP.

The seesaw pattern of winter intraseasonal precipitation anomaly was found between the southeastern CAWTP (centered in the Karakoram Himalaya) and the northwestern CAWTP (centered in the northern Pamir Plateau) by the SVD analysis and this pattern of precipitation was closely connected to the regional 700 hPa circulation. When there was a northeasterly moisture flux anomaly (southwesterly moisture flux weakened) over the northwestern CAWTP

and a southwesterly moisture flux anomaly (southwesterly moisture flux strengthened) over the southwestern CAWTP at 700 hPa, a negative precipitation anomaly occurred over the northern Pamir Plateau and a positive anomaly over the Karakoram Himalaya. Accompanied by the seesaw precipitation pattern, a negative 500 hPa geopotential height anomaly over CAWTP (center located in the central Tibetan Plateau) was also observed, and vice versa.

The mechanism for the seesaw precipitation anomaly over CAWTP may be related to the NAO-like circulation at the intraseasonal time scale. The results of both the regression and composite analyses showed that the seesaw precipitation pattern was closely connected with the precursor NAO-like circulation anomalies over the North Atlantic. During the positive NAO phases, the southern branch of the 700 hPa westerly winds formed a ridge over the North Atlantic and combined with the northern branch which formed a trough. The two branches separated around Eurasian border. The southern branch then formed a trough over the Middle East, which increased the transport of moisture and the strength of the westerly winds over the Karakoram Himalaya. By contrast, the northern branch formed a ridge and went around the northwestern Tibetan Plateau, which decreased southwesterly winds, the southwesterly moisture transport, and therefore precipitation over the Central Asia and northern Pamir Plateau. The large scale wind stream pattern can modify the regional circulation. Meanwhile during positive NAO, more WWD occurred over the Karakoram Himalaya since south branch of westerly encounters the Himalaya, which finally increased the precipitation over Karakoram Himalaya. This pattern was reversed during the negative NAO phases. The main physical processes involved and discussed above for the influence of the NAO on the winter

precipitation variability at the intraseasonal time scale over CAWTP are illustrated in schematic diagrams of Fig. 8.

Acknowledgments. This work was jointly supported by the National Key Research and Development Program of China (2016YFA0601904) and the National Natural Science Foundation of China (41572150, 41690115). BD's contribution was funded by the UK-China Research & Innovation Partnership Fund through the Met Office Climate Science for Service Partnership (CSSP) China as part of the Newton Fund. The authors would like to thank an anonymous reviewer and editor Xianan Jiang for their constructive comments on the earlier version of the paper.

LITERATURE CITED

Aizen E M, Aizen V B, Melack J M and others (2001) Precipitation and atmospheric circulation patterns at mid-latitudes of Asia. International Journal of Climatology 21: 535-556

Bjornsson H, Venegas S A (1997) A manual for EOF and SVD analyses of climatic data. CCGCR Report97: 112-134

Bothe O, Fraedrich K, Zhu X (2012) Precipitation climate of Central Asia and the large-scale atmospheric circulation. Theoretical and Applied Climatology108: 345-354

Cannon F, Carvalho L M V, Jones C and others (2015a) Multi-annual variations in winter westerly disturbance activity affecting the Himalaya. Climate Dynamics 44: 441-455

Cannon F, Carvalho L M V, Jones C and others (2015b) Winter westerly disturbance dynamics

401 and precipitation in the western Himalaya and Karakoram: a wave-tracking approach.
402 Theoretical and Applied Climatology: 1-18
403 Chen FH, Huang W, Jin LY, Chen J and others (2011) Spatiotemporal precipitation variations
404 in the arid Central Asia in the context of global warming.Science China Earth Sciences
405 54: 1812–1821
406 Chen M, Shi W, Xie P and others (2008) Assessing objective techniques for gauge–based
407 analyses of global daily precipitation. Journal of Geophysical Research: Atmospheres113:
408 D04110, doi:10.1029/2007JD009132
409 Curio J, Maussion F, Scherer D (2015) A 12-year high-resolution climatology of atmospheric
410 water transport over the Tibetan Plateau. Earth System Dynamics 6: 109-124
411 Dee D P, Uppala S M, Simmons A J and others (2011) The ERA–Interim reanalysis:
412 Configuration and performance of the data assimilation system. Quarterly Journal of the
413 Royal Meteorological Society 137: 553-597
414 Filippi L, Palazzi E, von Hardenberg J and others (2014) Multidecadal variations in the
415 relationship between the NAO and winter precipitation in the Hindu Kush–Karakoram.
416 Journal of Climate27: 7890-7902
417 Guo H, Chen S, Bao A and others (2015) Inter-comparison of high-resolution satellite
418 precipitation products over Central Asia. Remote Sensing 7: 7181-7211
419 Hoell A, Shukla S, Barlow M and others (2015) The forcing of monthly precipitation variability
420 over Southwest Asia during the boreal cold season. Journal of Climate28: 7038-7056
421 Hurrell, J W (1996) Decadal trends in the North Atlantic Oscillation: regional temperatures

422 and precipitation. Geophysical Research Letters 23: pp. 665–668
423 Lang T J, Barros A P (2004) Winter storms in the central Himalayas. Journal of the
424 Meteorological Society of Japan82: 829-844
425 Malik K M, Taylor P A, Szeto K (2015) Characteristics of moisture flux convergence in Central
426 Southwest Asia. Theoretical and Applied Climatology 120: 643-659
427 Mariotti A (2007) How ENSO impacts precipitation in southwest central Asia. Geophysical
428 Research Letters34:L16706, doi:10.1029/2007GL030078
429 Maussion F, Scherer D, Mölg T and others (2014) Precipitation seasonality and variability over
430 the Tibetan Plateau as resolved by the High Asia reanalysis. Journal of Climate27: 1910-
431 1927
432 Ozturk T, Altinsoy H, Türkes M and others (2012) Simulation of temperature and precipitation
433 climatology for the Central Asia CORDEX domain using RegCM 4.0. Climate
434 Research52: 63-76
435 Pohl E, Gloaguen R, Seiler R (2015) Remote sensing-based assessment of the variability of
436 winter and summer precipitation in the Pamirs and their effects on hydrology and hazards
437 using harmonic time series analysis. Remote Sensing7: 9727-9752
438 Ragab R, Prudhomme C (2002) Climate change and water resources management in arid and
439 semi-arid regions: prospective and challenges for the 21st century. Biosystems
440 Engineering 81: 3-34
441 Rana S, McGregor J, Renwick J (2017) Wintertime precipitation climatology and ENSO
442 sensitivity over central southwest Asia. International Journal of Climatology 37: 1494-

443 1509
444 Schiemann R, Lüthi D, Vidale P L and others (2008) The precipitation climate of Central
445 Asia—intercomparison of observational and numerical data sources in a remote semiarid
446 region. International Journal of Climatology28: 295-314
447 Schiemann R, Lüthi D, Schär C (2009) Seasonality and interannual variability of the westerly
448 jet in the Tibetan Plateau region. Journal of Climate 22: 2940-2957
449 Small E E, Giorgi F, Sloan L C (1999) Regional climate model simulation of precipitation in
450 central Asia: Mean and interannual variability. Journal of Geophysical Research:
451 Atmospheres104(D6): 6563-6582
452 Syed F S, Giorgi F, Pal J S and others (2006) Effect of remote forcings on the winter
453 precipitation of central southwest Asia part 1: observations. Theoretical and Applied
454 Climatology86: 147-160
455 Syed F S, Giorgi F, Pal J S, et al. (2010) Regional climate model simulation of winter climate
456 over Central–Southwest Asia, with emphasis on NAO and ENSO effects. International
457 Journal of Climatology30(2): 220-235
458 Wallace J M, Smith C, Bretherton C S (1992) Singular value decomposition of wintertime sea
459 surface temperature and 500-mb height anomalies. Journal of Climate5: 561-576
460 Wang N, Zhang Y (2015) Connections between the Eurasian teleconnection and concurrent
461 variation of upper-level jets over East Asia. Advances in Atmospheric Sciences32: 336-
462 348
463 WB, ISDR, CAREC (2009) Central Asia and Caucasus disaster risk management initiative

(CAC DRMI), Risk assessment for Central Asia and Caucasus. Desk study review: 1-155.http://www.preventionweb.net/files/11641_CentralAsiaCaucasusDRManagementInit.pdf (accessed 15 Sep 2016)

Yadav R K, Rupa Kumar K, Rajeevan M. (2009) Increasing influence of ENSO and decreasing influence of AO/NAO in the recent decades over northwest India winter precipitation. Journal of Geophysical Research: Atmospheres 114(D12)

Yao J, Chen Y. (2015) Trend analysis of temperature and precipitation in the Syr Darya Basin in Central Asia. Theoretical and Applied Climatology 120(3-4): 521-531

Yin ZY, Wang HL, Liu XD (2014) A comparative study on precipitation climatology and interannual variability in subtropical East Asia and Central Asia. Journal of Climate27: 7830-7848

476 Table 1 Correlation coefficients of regionally-averaged 500 hPa geopotential heights on
477 different lead-lag days for four regions indicated in Fig. 5 with the time coefficients of the
478 first mode of 500 hPa geopotential height field over CAWTP in the SVD analysis mentioned in
479 the text, and the correlation coefficients between NAO index and the time series. A negative
480 lag means that the regionally-averaged height value over the four regions leads the height
481 anomaly over CAWTP in the SVD analysis.

Lag day	Area A	Area B	Area C	Area D	NAOI
-16	0.13	-0.14	-0.06	-0.15*	0.19**
-15	0.16*	-0.22**	-0.01	-0.20**	0.22**
-14	0.17*	-0.23**	0.02	-0.24**	0.24**
-13	0.15*	-0.24**	0.04	-0.26**	0.24**
-12	0.14	-0.30**	0.07	-0.29**	0.23**
-11	0.13	-0.33**	0.11	-0.30**	0.21**
-10	0.15*	-0.30**	0.11	-0.32**	0.20**
-9	0.17*	-0.32**	0.11	-0.35**	0.20**
-8	0.14	-0.36**	0.10	-0.38**	0.21**
-7	0.13	-0.44**	0.11	-0.41**	0.20**
-6	0.17*	-0.48**	0.16	-0.44**	0.16*
-5	0.20**	-0.46**	0.26**	-0.47**	0.12
-4	0.17*	-0.46**	0.39**	-0.51**	0.08
-3	0.14	-0.40**	0.54**	-0.59**	0.05
-2	0.14	-0.34**	0.67**	-0.68**	0.04
-1	0.16*	-0.23**	0.70**	-0.75**	0.04
0	0.15*	-0.17*	0.67**	-0.67**	0.00
1	0.12	-0.16*	0.59**	-0.57**	-0.08
2	0.08	-0.06	0.48**	-0.47**	-0.14
3	0.05	-0.03	0.44**	-0.39**	-0.14

482 *Significant at the 95% level **Significant at the 99% level

483

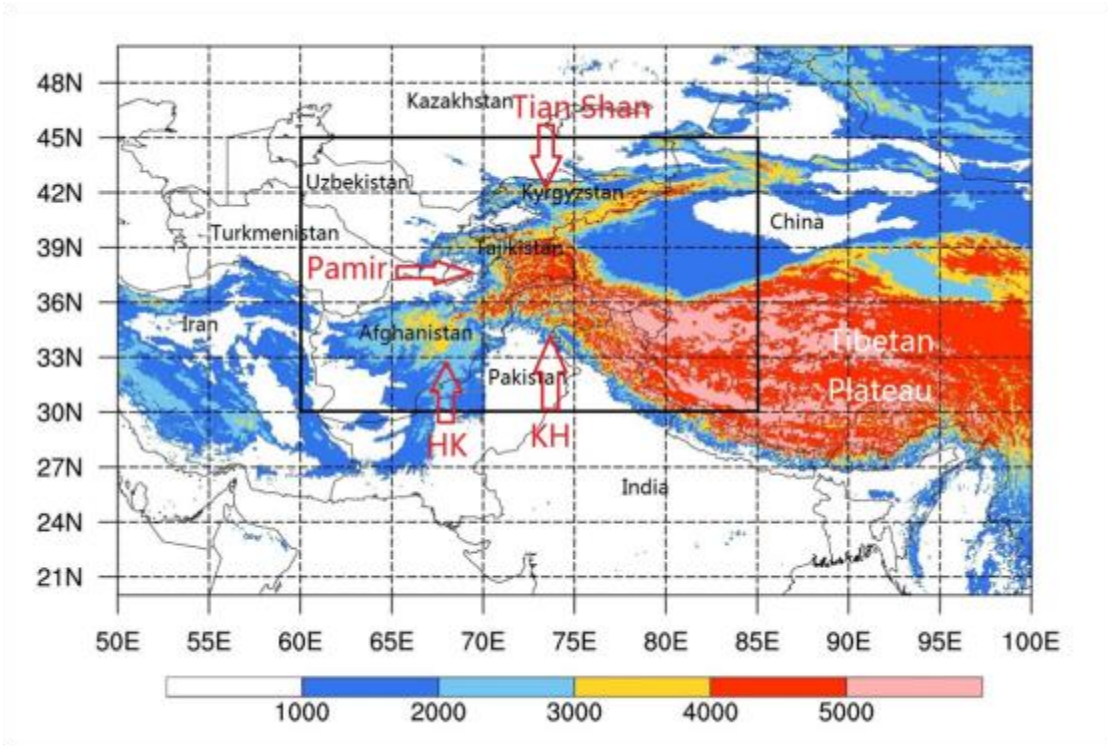

Fig. 1. Topography (color shaded areas, in meters) and national boundaries (thin gray lines) of Central Asia, the western Tibetan Plateau (outlined by the black box) and surrounding areas. HK and KH indicate Hindu Kush and Karakoram Himalaya, respectively.

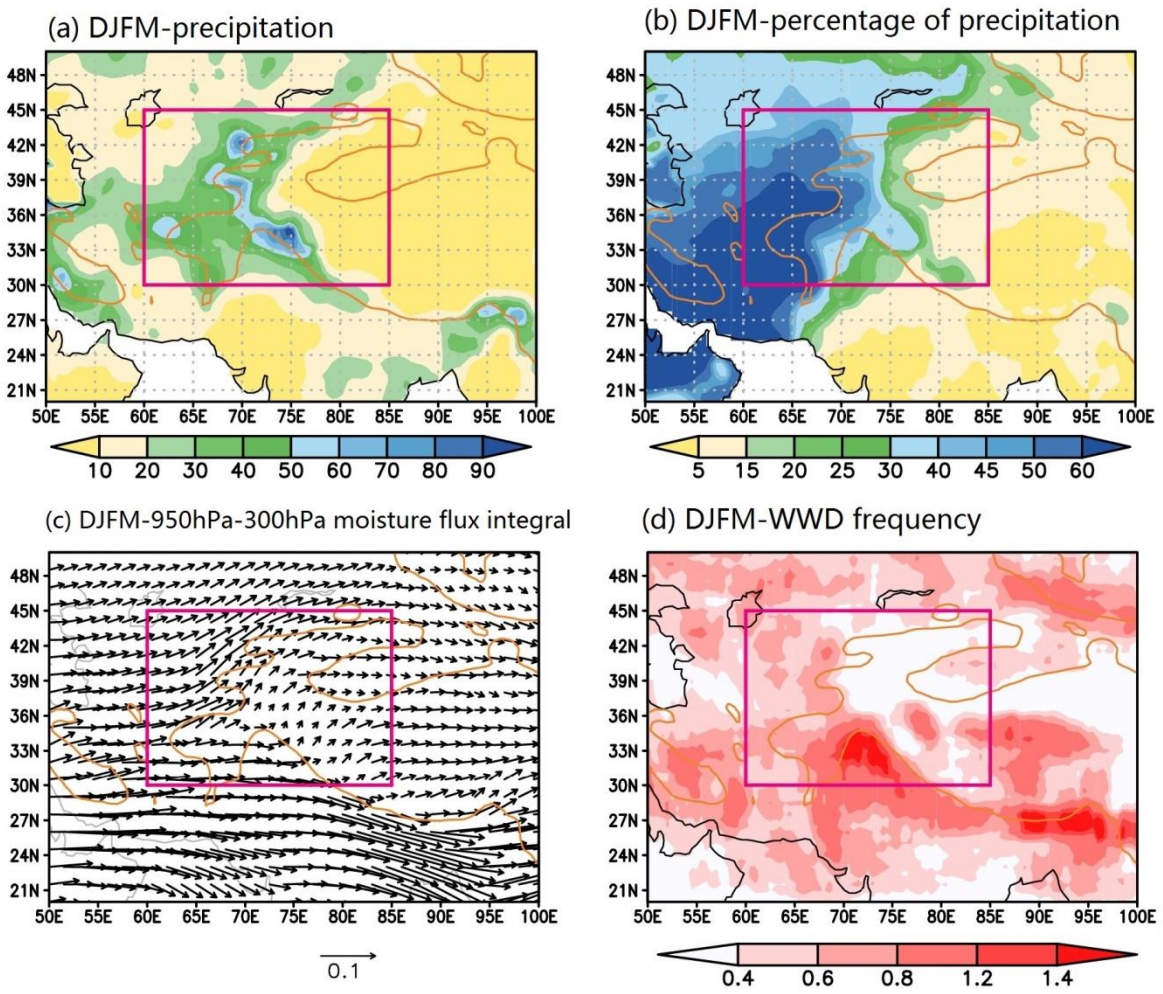

Fig. 2. (a) Average precipitation (0.1 mm d^{-1}), (b) percentage of annual precipitation falling in winter (%), (c) water vapor flux integrated vertically for 950–300 hPa (kg m^{-1} s^{-1}) and (d) westerly wind disturbances frequency (percentage per day) in the CAWTP and surrounding areas in winter (December-March) for 1979–2013. The brown lines indicate the topographic contour of 1500 m and the red boxes represent the CAWTP region.

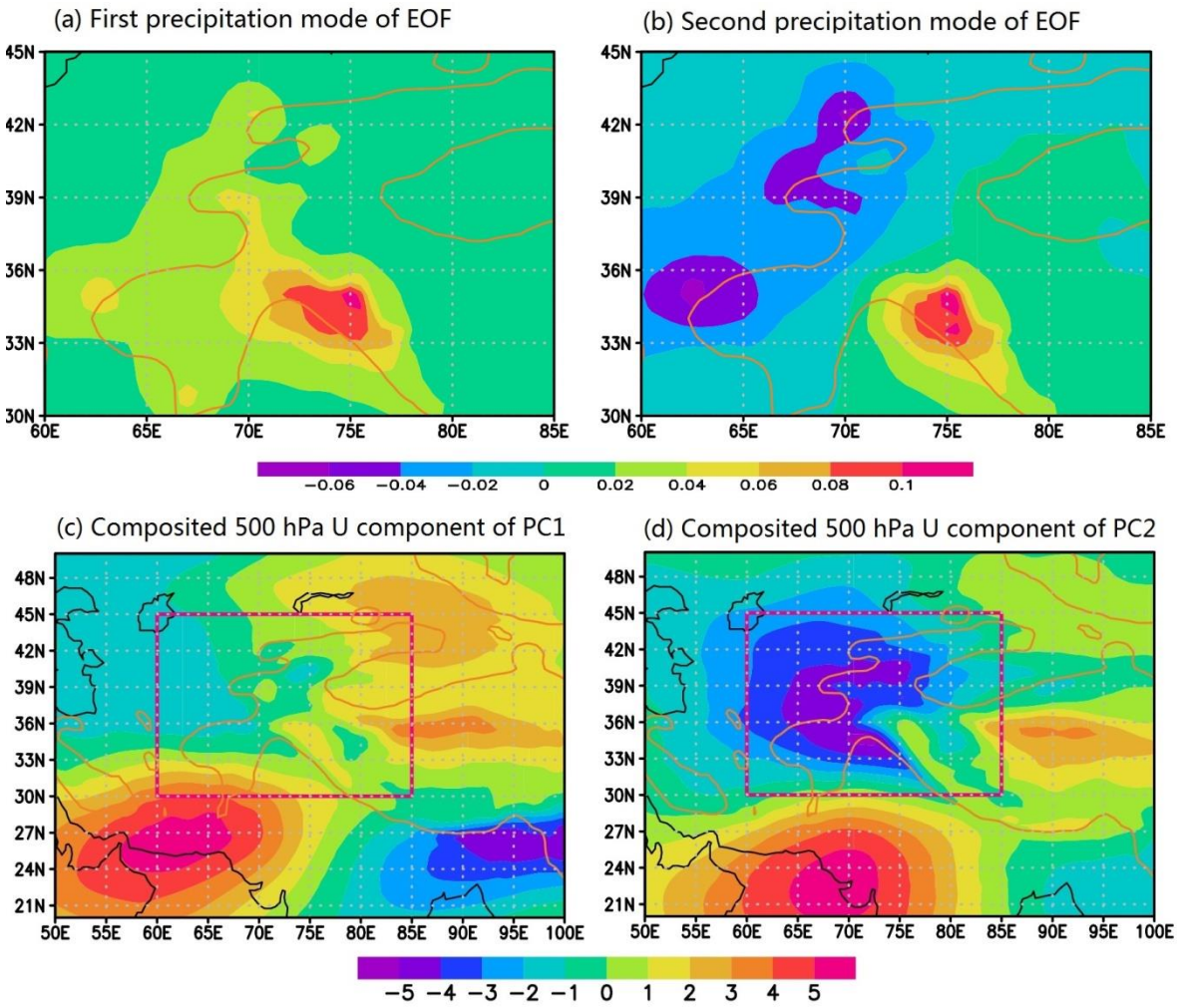

494

495 Fig. 3. First mode (a) and second mode (b) of the EOF analysis of daily precipitation field for
496 winters during 1979-2013. The composited 500 hPa zonal wind (U component) of the
497 dominant periods of the First mode (c) and second mode (d). The brown lines represent the
498 topographic contour of 1500 m.

499

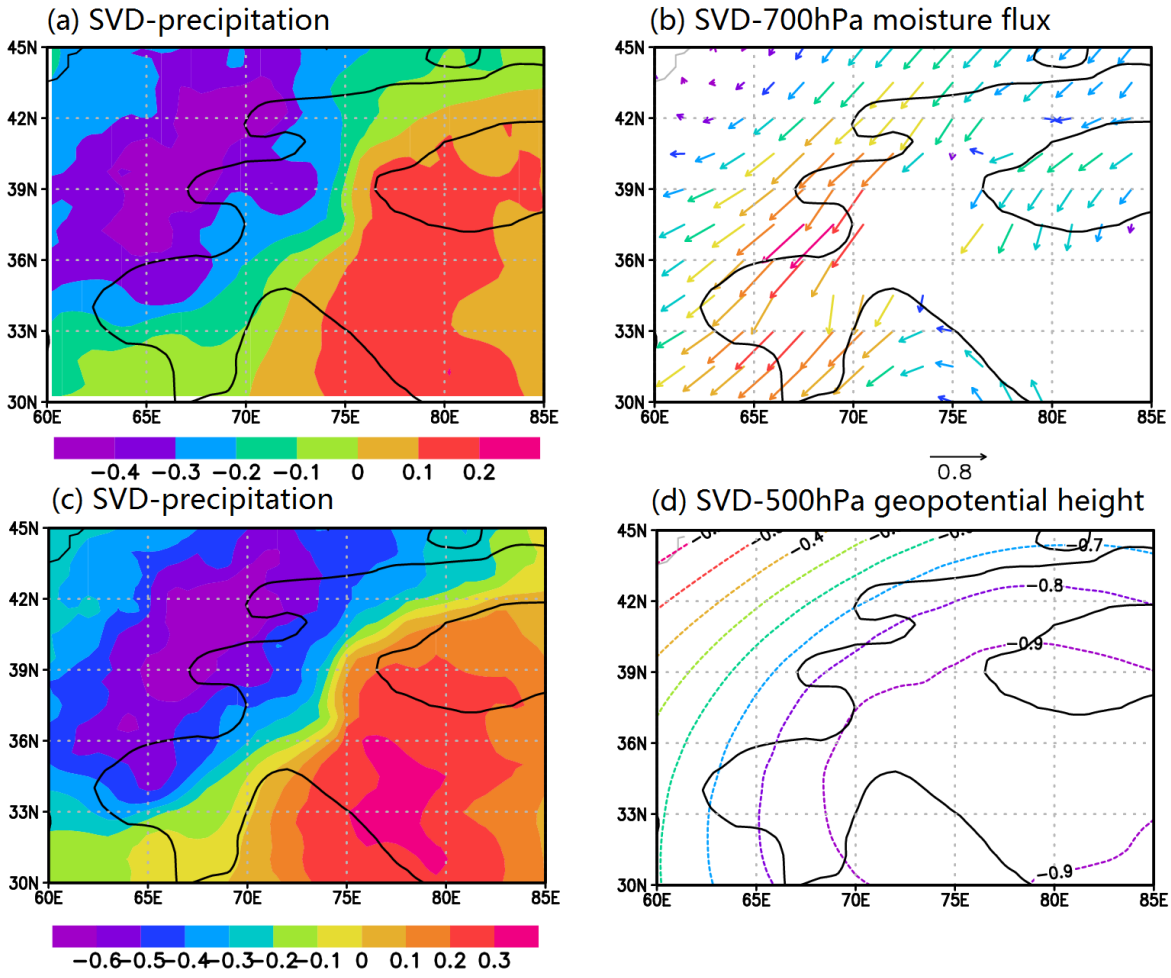

Fig. 4. First mode of the SVD analysis between seasonal cycle removed daily precipitation field (a) and 700 hPa daily moisture flux field (b) for winters during 1979-2013. Panels (c) and (d) are the same as (a) and (b), respectively, but for precipitation field (c) and 500 hPa geopotential height field (d). The black lines represent the topographic contour of 1500 m.

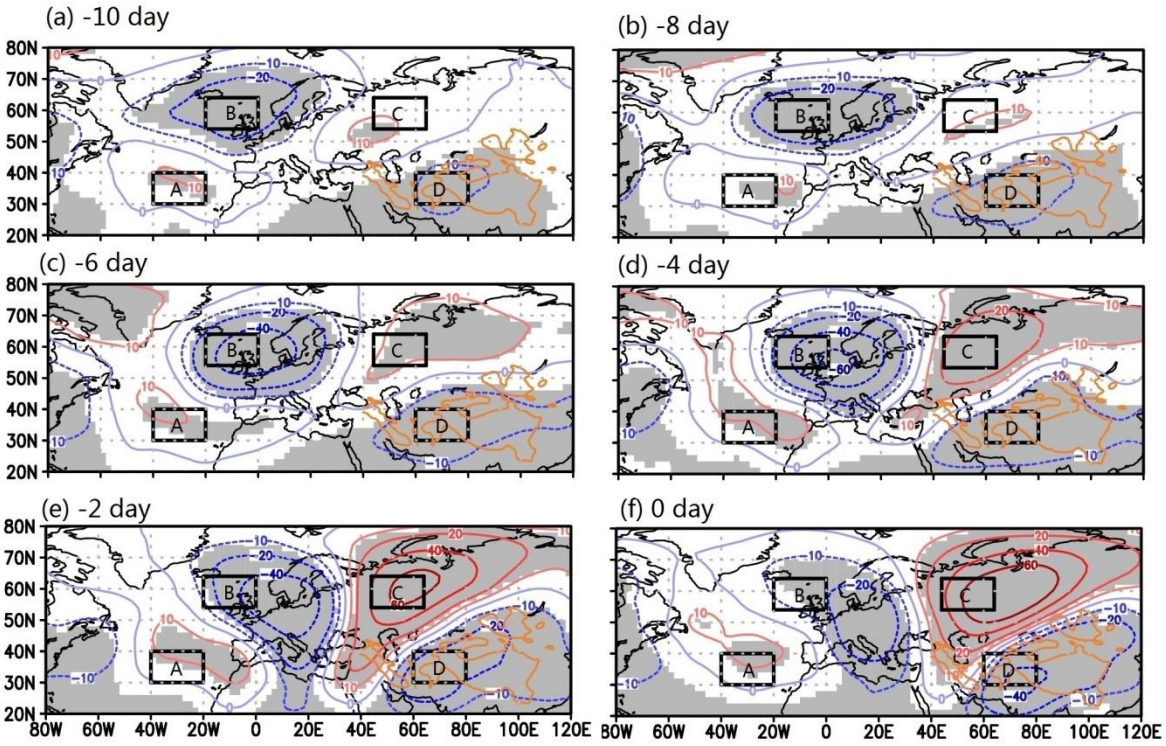

507

508 Fig. 5. Regressed 500hPa geopotential height anomaly fields for days (a) −10, (b) −8, (c) −6, (d)
509 −4, (e) −2 and (f) 0 with the chosen 200time coefficients of the first mode of 500 hPa
510 geopotential height field over CAWTP in the SVD analysis. The negative value indicates the
511 number of days before the day of SVD analysis. The contours represent the regression
512 coefficients and the gray shading represents the areas that were significant at the 95% level.
513 The brown lines represent the 1500 m topographic height and the black boxes represent the
514 four geopotential height anomaly centers.

515

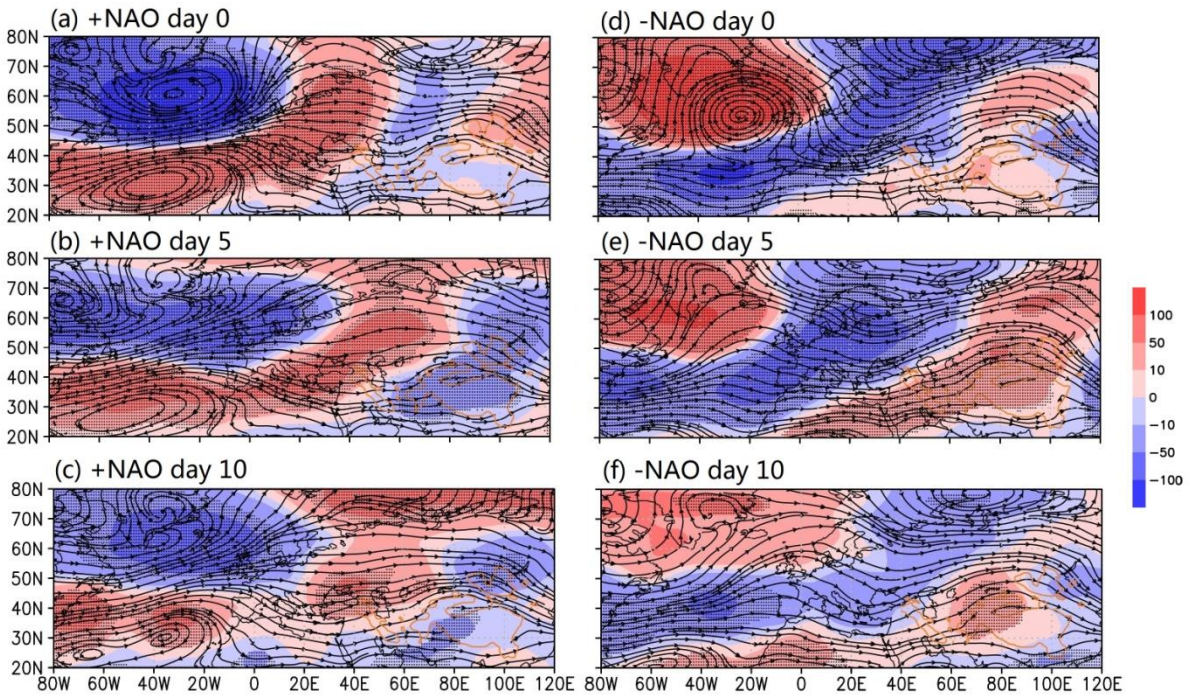

516

517 Fig. 6. The 500 hPa geopotential height anomaly (in potential meters) and 700 hPa wind
518 stream line averaged on the peak day (day 0), day 5 and lag day 10, composited for 85 positive
519 NAO events (a, b and c) and for 82 negative NAO events (d, e and f). The brown lines represent
520 the 1500 m isoheight. The dots represent the grid points where the 500 hPa geopotential
521 height anomaly were significant at the 95% significance level.

522

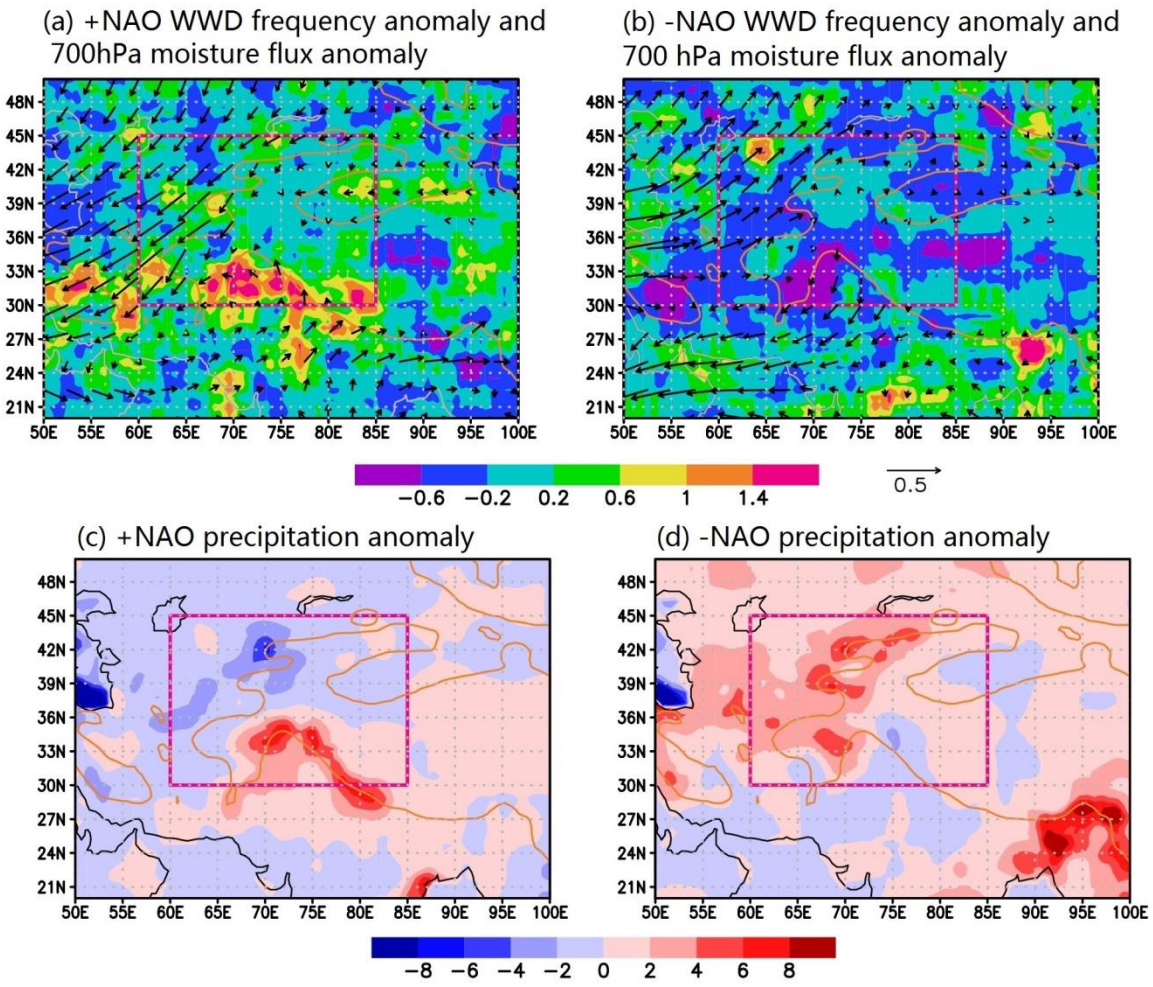

523

524 Fig. 7. The 700 hPa moisture flux anomaly (g $s^{-1}hPa^{-1}cm^{-1}$, vectors) averaged from +5 day (5
525 days after the peak day) to the +10 day and WWD frequency anomaly (percentage per day,
526 shaded), composited for 85 positive NAO events (a) and for 82 negative NAO events (b). Panels
527 (c) and (d) are the same as panels (a) and (b), respectively, but for precipitation anomaly (in0.1
528 mm d^{-1}).The brown lines represent the 1500 m isoheight and the red boxes represent the
529 CAWTP region.

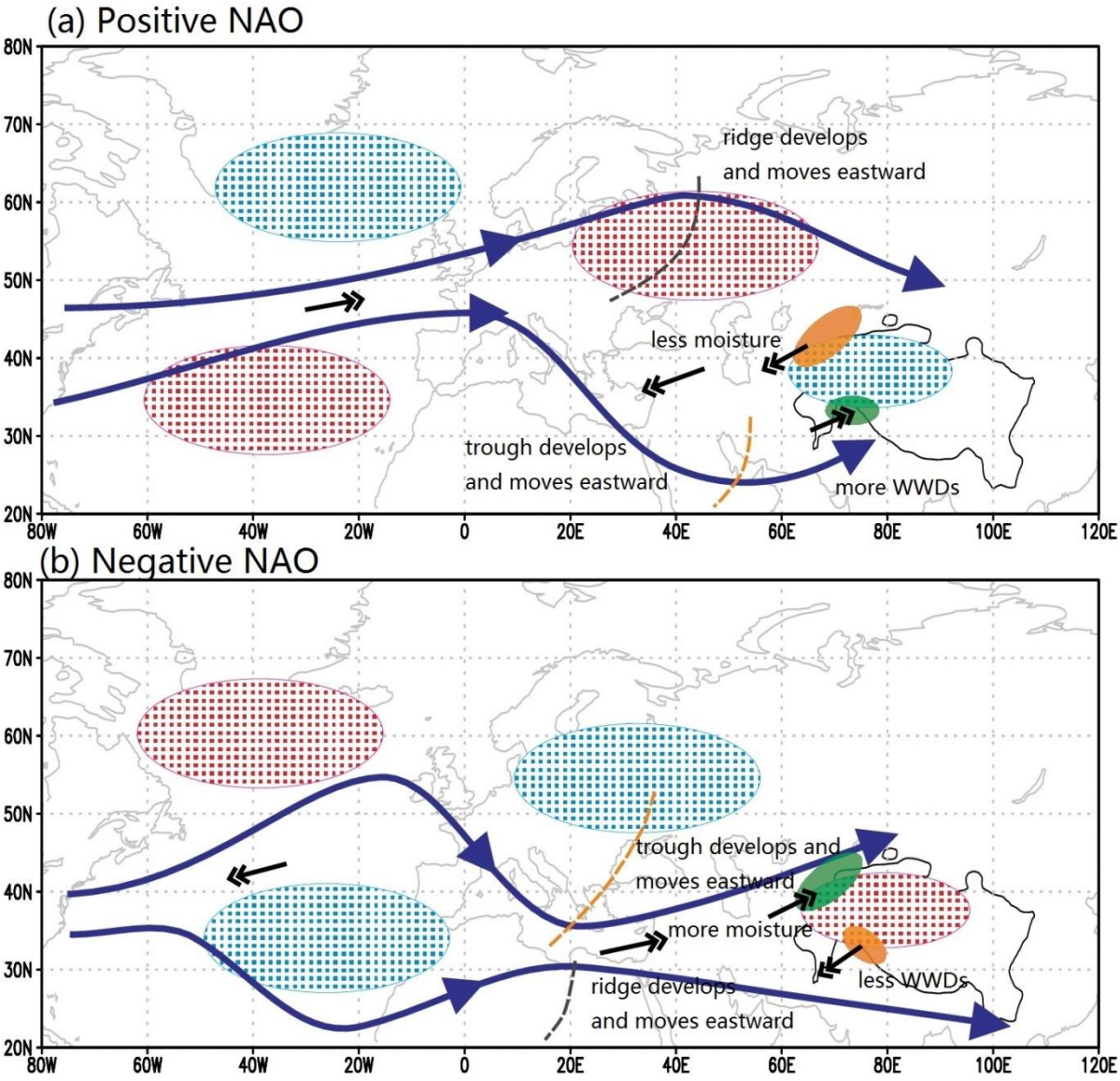

Fig. 8. Schematic diagrams showing how positive (a) and negative (b) NAO events influence the precipitation over the CAWTP region. The red and blue ellipses are the areas of the 500 hPa positive and negative geopotential height anomalies. The blue lines represent the southern and northern branches of the 700 hPa westerly circulation. The black arrows represent the 700 hPa wind anomaly. The brown and gray dotted line represent troughs and ridges. The green and yellow areas represent the positive and negative precipitation anomalies.